Impact of acetylation process of kraft lignin in development of environment-friendly semisolid lubricants

M. Trejo-Cáceres, M. Carmen Sánchez, J.E. Martín-Alfonso*

Department of Chemical Engineering and Materials Science, Campus de El Carmen, University of Huelva, Chemical Product and Process Technology Research Center (Pro^{2}TecS). 21071 Huelva. Spain.

* Corresponding author. Present address: Department of Chemical Engineering and Materials Science, 21071 Huelva, Spain. Tel.: +34 959218204.
E-mail address: jose.martin@diq.uhu.es (J.E. Martín-Alfonso)

ABSTRACT

The aim of this work was to study the influence of the acetylation process of kraft lignin on developing dispersions potentially applicable as new bio-based semisolid lubricants. Lignin was functionalized with acetic anhydride and pyridine as a catalyst by modifying different reaction variables (temperature, ratio of pyridine/acetic anhydride and time). Acetylated lignin was analyzed using FTIR, ^{1}H and ^{13}C NMR techniques, TGA, DSC and SEM to evaluate the chemical, morphological and thermal changes induced by the acetylation process. The influence of the acetylation process on the rheological and tribological properties of dispersions was related to the development of different microstructures, which depend on chemical and morphological properties of acetylated lignin. In this sense, two different rheological behaviours (gel-like or fluid-like) were found to depend on the reaction time. From the experimental results obtained, it can be concluded that the acetylation process is a key issue to modulate rheological and morphological properties of dispersions, resulting in an effective method to improve the compatibility of lignin and castor oil. Acetylated lignin with medium degrees of substitution with adequate morphological properties can be potentially used as an effective thickening agent to develop semisolid lubricants.

Keywords: Lignin, acetylation process, bio-lubricant, rheology, tribology

1. Introduction

Today, there is an increased evolution in the usage of non-toxic and natural products toward renewable resources in order to diminish the negative effects that process technologies and products cause to human health and the environment [1]. In connection with this, the lubricant industry has been making some efforts to develop sustainable lubricants, both liquids and semi-solids, for several years [2-4]. Semisolid lubricants (such as greases) are generally highly structured colloidal dispersions that possess a two-phase structure consisting of a thickener agent (traditionally metallic soaps or polyurea compounds) and a fluid oil lubricant (generally mineral or synthetic). The thickener forms a colloidal network, which traps the oil in its micro-nano structure and allows the grease to exist in the semisolid state [4]. The replacement of traditional thickeners by more environmentally friendly constituents faces many more challenges than the substitution of non-biodegradable lubricants fluid by vegetable oils or their derivatives because the thickener must form an adequate entanglement network trapping the oil and must confer appropriate functional properties, such as gel-like behavior, thermal resistance or lubrication efficiency. Hence, the search of novel thickener agents or approaches to develop sustainable semisolid lubricants is a cutting-edge topic in lubricant industry, as it is a very attractive subject from economic, social, and environmental standpoints. Recently, the use – and therefore the valorization – of lignin as a high-added-value chemical precursor to develop additives and thickener agents for lubricant purposes has been investigated with promising results [5-7]. Lignin is a three-dimensional amorphous aromatic polymer, built up from structural units such as guaiacyl (G-units), syringyl (S-units), and phydroxyphenyl (P-units), which are derivatives of coniferal, synapyl, and pcoumaryl alcohols, respectively [8, 9]. These molecular units are linked by various types of ether (C-O-C) and carbon-carbon (C-C) bonds to form a three-dimensional structural network [10]. The chemical structure and properties of lignin are greatly dependent on

the biomass feedstock and/or on the pretreatment procedure [11]. According to the development of semisolid lubricants, lignin presents several advantages compared to metallic soaps, since it is an environmentally friendly material with a small environmental footprint and is obtained from renewable sources. Moreover, lignin, after cellulose, is the second most abundant biopolymer on the planet, constituting about 15–25% of the total dry weight of woody plant material. The pulp and paper industries produce between 40 and 50 million tons of lignin each year, but only 2% are used for the production of value-added materials [12]. In addition, its unique phenolic structure makes it an excellent antioxidant additive to limit the physicochemical degradation of lubricant oil during its use in rolling-bearing applications [13]. Nevertheless, it has a significant inherent disadvantage, mainly associated with its poor ability to form physically stable gel-like dispersions in oil media. This effect results from its numerous OH groups, which restrict its dispersibility in oil. However, this can also be an asset, since these OH groups can ideally be used as a platform to make chemical modifications. Their derivatization and subsequent functionalization can help decrease the hydrophilic character, thus improving lignin's compatibility with oil and minimizing the limitations regarding the physical stability under static conditions. The most common reactions used to enhance the miscibility of lignin with other non-polar media, especially with polyolefins are alkylation [14, 15], silylation [16], esterification [17-19] and epoxidation [7]. Among the different modification routes, the chemical modification of the hydroxyl groups through an esterification process is a promising approach for the functionalization of lignin, since this reaction is widely used for the modification of lignocellulosic sources [20, 21]. The acetylation reaction is usually performed in the liquid phase using acetic anhydride and pyridine as the esterification agent and the catalyst, respectively [16, 22, 23]. Acetylation of lignin has been recently studied via several approaches. Shayesteh et al. [24] studied and optimized same parameters that affect the acetylation of sulfonate lignin using acetic

anhydride, while Rabelo de Oliveira et al. [25] demonstrated that partial and selective acetylation of kraft lignin can be carried out through a simple and fast microwave-assisted process using acetic acid as both the solvent and acetylating agent. However, these studies were conducted after a successful synthesis of the lignin without providing a subsequent in-depth exploration of the applicability of the material. Thus, it is reasonable to say that there have yet been no proposed and explored extensive works focusing on the development of dispersions based on acetylated lignin and vegetable oil. It is expected that the highly reactive hydroxyl groups in the chemical structure of lignin will lead to an increase in the modification efficiency, improving the properties of the final dispersions, which could drive potential innovative applications in fields such as the lubricant or bitumen industries. Taking into account these considerations, the objective of this work was to study the role of the acetylation process of kraft lignin in the development of dispersions potentially applicable as environmentally friendly semisolid lubricant formulations. In order to achieve this goal, lignin was reacted with acetic anhydride in the presence of pyridine as a catalyst. The influence of three reaction variables such as temperature, ratio of pyridine/acetic anhydride and reaction time on chemical, morphological and thermal properties of modified lignin and rheological/tribological properties of resulting dispersions in castor oil was studied. This work may serve as a starting point to develop a deeper understanding of the acetylated lignin and its impact on the rheological and tribological properties of vegetable oil dispersions and might pave the way for further application of these bio-based products.

2. Materials and methods

2.1 Materials

Softwood kraft lignin (KL, M_w: ~10,000 g/mol) [26], acetic anhydride, pyridine and hydrochloric acid were purchased from Merck Sigma-Aldrich. All chemicals were

reagent grade and used without any further purification. Castor oil (211 cSt at 40 °C, Guinama, Spain) was used as biodegradable oil media to prepare dispersions with acetylated kraft lignin.

2.2 Preparation of acetylated kraft lignin and dispersions

The acetylation of kraft lignin was conducted via acetic anhydride, catalyzed by pyridine, according to the method described by Shayesteh et al (2020) [24]. Pyridine was chosen as a catalyst for this reaction due to its high catalytic activity [27], small dosage, and lower amount of waste product. **Fig. 1** illustrates the proposed acetylation mechanism catalyzed by pyridine of alcohol (aliphatic and aromatic) with acetic anhydride. Initially, the nitrogen atom in the pyridine ring attacks the carbonyl of acetic anhydride to form an ion pair of acetate and *N*-acetylpyridinium (**Fig 1a**). Then, the esters were obtained from acetic anhydride and alcohol-catalyzed by pyridine through the following two pathways. In the first way, the aromatic alcohol is added to the *N*-acetylpyridinium and forms an ester and a deactivated (protonated) catalyst (**Fig. 1b**). The last step is the rate determining step. In the second way, an aliphatic alcohol is added to the C-O double bond of acetic anhydride through a four-membered or six-membered-ring transition state with pyridine, and then an ester is generated (**Fig. 1c**). The formation of a four-membered-ring or six-membered-ring transition state is the rate-determining step [28]. In a typical procedure, 2 g of kraft lignin was added to a mixture of acetic anhydride and pyridine, in a round-bottomed flask immersed in an oil bath to control temperature, by modifying three reaction variables: temperature (10-60ºC), ratio of pyridine/acetic anhydride (0:1, 1:1, 1:2, 1:3, 1:4, 1:5) and time (1-72 h). The values of ratio of pyridine/acetic anhydride were selected according to previous work carry out by Shayesteh et al. [24]. Lignin and pyridine were dissolved in a 100 mL flask, and acetic anhydride was added. An excess of acetic anhydride was added to

favor the formation of acetylated products in the chemical equilibrium. Then the reaction mixture was stirred at controlled temperature. Finally, 10 volumes of HCl (0.1 M) were added at around 5ºC, and acetylated lignin was filtered through a Brinell funnel and washed with distilled water to a neutral pH. The acetylated kraft lignin was dried in a vacuum oven at 50°C for 24 h. Each experiment was performed four times to ensure the repeatability of the results. To prepare dispersions, acetylated lignin was dispersed in castor oil using a laboratory scale mixing device fitted with an anchor impeller geometry at room temperature (around 23 ºC), and a rotation speed of 60 rpm during 60 min, employing lignin concentrations in the range of 30-40 wt.%.

2.3 Characterization of kraft lignin and acetylated samples

The physicochemical and morphological changes of lignin were analyzed before and after the esterification process. Fourier transformed infrared spectroscopy (FTIR) spectra of lignin was obtained using a typical KBr method with a JASCO FT/IR-4200 spectrometer after the samples were purged with nitrogen. Each sample was scanned 46 times at a resolution of 4 cm^{-1} over the wavenumber region of 4000–400 cm^{-1}.

Proton and carbon nuclear magnetic resonance (^{1}H NMR and ^{13}C NMR) spectra were acquired at room temperature on a Bruker Avance III 500 MHz spectrometer. For analysis, about 25 mg of lignin or acetylated lignin were dissolved in 0.6 mL DMSO-d_6. The proton and carbon NMR spectra were acquired using 32 and 9000 scans, spectral widths of 12 ppm and 185 ppm and frequencies of 500MHz and 125 MHz for ^{1}H and ^{13}C, respectively. The DMSO-d_6 solvent was used as the internal reference ($^{1}H/^{13}C$, 2.5-39.3 ppm). The morphological characteristics were observed using scanning electron microscopy with a FlexSEM 1000 II microscopy, after sputtering the samples with gold under vacuum, operating at 5 kV acceleration voltage and 20 mm working distance.

Thermal behavior was characterized via dynamic scanning calorimetry (DSC) and thermogravimetric analysis (TGA). DSC analyses were carried out on a TA Instruments model Q-100, in a temperature range of -75 to 220 °C for glass transition determination at a scan rate of 10 °C/min under a nitrogen atmosphere, while TGA was performed on a TA Instruments model Q-50 with a heating rate of 10 °C/min from 30 to 600 °C under a nitrogen flow of 50 mL/min.

2.5 Rheological and tribological measurements of dispersions

The rheological tests were performed by a Rheoscope controlled-stress rheometer at 23 °C, using a rough plate–plate geometry (20 mm diameter and 1 mm gap), to prevent possible slip phenomena. For Small-Amplitude Oscillatory Shear (SAOS) tests, the stress sweep was completed at 6.28 rad/s to determine stress values within the linear viscoelastic region. The frequency sweep in the frequency range of 0.03 to 100 rad/s was subsequently performed. In the steady shear test, the measurements were performed at shear rates from 0.01 to 100 s^{-1}, collecting the viscosity data every 2 min once the apparent viscosity had reached steady-state values at the applied shear rate. Tribological performance of dispersions was investigated on a Modular Compart Rheometer (MCR-501, Anton Paar) with a tribological cell coupled with a tribological ball-on-three-plate testing module. The three lower plates (made from 1.4301 steel) were fixed through the sample holder forming 45º to the rotating axis, and the upper ball (made from 1.4401 steel) was placed on with a pre-set normal load applied. The friction coefficient was obtained by applying a normal load of 20 N and a constant rotational speed of 100 rpm during 650 s at 23ºC. This test was repeated four times to obtain an accurate average friction factor. For each test, new ball and plates contact areas were used, and all specimens were cleaned with ethanol. A standard Olympus BX51 microscope (Olympus Optical, Japan) was employed to look at the wear marks and measure the wear scar diameter (WSD).

3. Results and discussion

3.1 Influence of acetylation process on chemical, morphological and thermal properties of kraft lignin

The FTIR was the first technique that was used to evaluate the chemical modification of kraft lignin after the esterification process. **Fig. 2** shows the infrared spectra of neat lignin and acetylated lignin at a reaction temperature of 30 °C and a ratio of pyridine/acetic anhydride (1/3) as a function of reaction time. As can be observed, neat kraft lignin displays peaks at 1600, 1510, 1457, and 1424 cm^{-1} corresponding to aromatic skeleton vibrations, and are typical lignin absorptions [29, 30]. The peak at 3420 cm^{-1} corresponds to O-H stretching of phenolic hydroxyl vibrations, and the peaks at 2930 and 2845 cm^{-1} could be attributed to methyl and methylene groups. The peaks at 1264 and 812 cm^{-1} correspond to C-H plane vibrations of guaiacyl (G- units), while the peak at 1221 cm^{-1} was attributed to C-O-C of G-units. In addition, the peak at 1132 cm^{-1} was assigned to C-H of syringyl (S-units) [28]. Both G- and S-units are present at 1078 cm^{-1} [31]. Regarding the spectra of acetylated samples, the presence of a new band with two peaks at 1740 and 1760 cm^{-1} corresponding to aliphatic and aromatic C=O ester groups, respectively, and the peak at 1200 cm^{-1} was attributed to C-O-C of aromatic acetyl groups. They corroborated the successful acetylation of lignin [17, 18] (see **Fig. 2b**). The peaks at 1600, 1510, 1457, and 1424 cm^{-1} corresponding to aromatic skeleton vibrations showed no change. This indicated that the main structure of lignin did not change during acetylation process. The peak at 1370 cm^{-1} corresponded to plane vibrations of the C-H stretching of the acetate methyl group, and the intensity increased with the reaction time. All the latter peaks are summarized in **Table 1.** Another change of the acetylated samples in the infrared spectrum is the modification in the shape and intensity of the band between 3700 and 3000 cm^{-1}, with a maximum around 3400 cm^{-1}, characteristic of O−H stretching

of phenolic or aliphatic units. As can be clearly observed, this band decreased when the reaction time increased, thus providing a measure of the advance of the chemical reaction. In this sense, the calculation of the degree of substitution (DS) was carried out through the FTIR results as a measure to quantify the chemical modification degree of lignin [19, 25]. The absorbances assigned to -OH stretch vibration (A_{OH}) were measured and normalized with respect to the band at 1510 cm^{-1} (A_{ref}). According to the literature, the band at 1510 cm^{-1} is one of the characteristic bands assigned to aromatic skeletal vibrations of lignin [32]. This band is well defined in neat lignin and acetylated samples spectra. It could thus be used to normalize the area. Thus, the substitution degree in acetylated samples can be calculated as follows:

$$DS = 1 - \left[\frac{(A_{OH} - A_{ref})_{acetylaed\ lignin}}{(A_{OH} - A_{ref})_{neat\ lignin}}\right] \times 100 \quad (1)$$

Based on this expression, the DS of acetylated samples was estimated in order to determine the effects of three variables studied on the esterification process. The influence of these variables on DS is shown in the **Fig. 3**. As can be seen, all acetylated samples show values of the average number of sites per OH unit of the lignin molecule on which there are acetyl groups comprised between 53% and 91%. As previously mentioned, this fact could be related to a significant decrease in the ratio of the hydroxyl group and the appearance of the acetylation of phenolic and aliphatic hydroxyls due to adequate reaction parameters. According to **Fig. 3a**, when the temperature increases from 10 to 30ºC, the DS increases, while the normalized area of hydroxyl group decreases. It is known that an increase in the reaction temperature leads to the dissociation of the hydrogen bonds within the lignin structure and to a higher reaction rate [22]. However, higher temperatures (> 30ºC) provide lower DS values, particularly at 60ºC. This fact could be attributed to a chemical shift in the reaction toward the deacetylation process, as well as to the

weakening of molecular bonds of the acetyl group, increasing its dissociation from the lignin. Similar behavior was observed when the ratio of pyridine/acetic anhydride increased (see **Fig. 3b**). The increase of the ratio of the pyridine/acetic anhydride up to 1:3 had a positive effect on the progress of the acetylation reaction. However, its further increase has a reverse effect on the acetylation reaction process [33]. This may be due to the fact that the reaction medium is saturated with ions acetate and *N*-acetylpyridinium, increasing the probability of formation of acetic anhydride vs the formation of acetates by reaction with the alcohols (aliphatic and aromatic) in lignin (see **Fig. 1**). Also notably, the absence of the catalyst (ratio 0:1) leads to a high DS for these reaction conditions. This could be attributed to the fact that once the acetylation reaction begins, it detaches the acetic acid as product, and its presence could catalyze the chemical reaction of lignin. Similar results were found by Cachet et al [34] for esterification of organosolv lignin under supercritical conditions. Nevertheless, Shayesteh et al. [24] observed a certain acetylation degree of lignin by the carbonyl group without any amount of pyridine. Nevertheless, the hydroxyl group was similar to neat lignin and concluded that the acetylation was not performed. As can be seen in **Fig. 3c**, an increase in reaction time from 1 h to 12 h resulted in an increase in DS, from 53 to 92%, while from 12 h to 72 h, the DS remained roughly constant or slightly decreased. An increment of DS with the reaction time is a consequence of the favorable effect of time on diffusion and adsorption of the reactants, which leads to better contacts between the acetic anhydride and the lignin particles [16]. Acetylation was relatively fast during the first 12 h, suggesting that easily accessible hydroxyl groups were first modified. After 12 h, the reaction rate slowed down, and the reaction receives a chemical-shift again. Since it is known that long reaction times favor the cleavage of ether bonds present in the lignin structure, this reverse reaction toward the reactants begins competing with the forward acetylation reaction to a notable degree [25]. In summary, it may be concluded that an increase of three variables studied

on the acetylated reaction increases the DS up to values that depend on the relationship between their other counterparts. Then, a roughly constant or slightly decrease of DS occurs, associated with the increased rate of the reverse process(deacetylation). The chemical structures of neat lignin and acetylated samples were also analyzed by ^{1}H NMR and ^{13}C NMR, shown in **Fig. 4** as a function of reaction time. The chemical structures of neat lignin and acetylated samples were also analyzed by ^{1}H NMR and ^{13}C NMR, as shown in **Fig. 4,** as a function of reaction time. For the kraft lignin, peaks at 1.23, 3.50–4.10, 3.00–3.50, and 8.50 ppm corresponding to the alkyl, methoxyl (-OCH_3), aliphatic hydroxyl, and phenolic hydroxyl groups, respectively, can be observed in the proton spectrum (**Fig. 4a**) [35]. In the range of aromatic hydrogens (6.0–7.5 ppm), the characteristics of three phenyl propane units were distinguishable for the appearance of peaks at 6.0–6.8, 6.8–7.0, and 7.0–7.5 ppm, corresponding to aromatic protons in the syringyl (S-units), guaiacyl (G-units), and positions 2 and 6 of the H units conjugated with a double bond, respectively. The appearance of peaks at 6.0-5.8 ppm corresponding to H_α and H_β of β-O-4 that β-carbon in one phenyl propane unit connected with 4-carbon in another phenyl propane unit by ether linkage, respectively, indicated that there were a lot of β-O-4 connections in lignin [28]. For the acetylated samples, the acetylation was confirmed to be successful by the following changes. First, strong peaks at 1.70–2.45 ppm, corresponding to -CH_3 ester (1.70−2.10 ppm aliphatic -CH_3 ester and 2.10−2.45 ppm phenolic -CH_3 ester) [36]. Second, the peaks at 3.0-3.5 ppm of the aliphatic hydroxyl disappeared for acetylated samples. However, they came back again for the higher reaction times (48 and 72 h), associated with the reversibility of acetylation reaction. In addition, the peak at 8.50 ppm related to the phenolic OH protons was not observed in the spectrum, demonstrating the conversion of most of the phenolic OH groups to their acetylated form and that phenolic OH groups react more easily than their aliphatic counterparts [16]. Third, the aromatic hydrogen does not vary during esterification.

Furthermore, the integration area of 1.70–2.10 ppm corresponding to aliphatic -CH_3 ester increased up to a maximum (24 h), while the area of 2.10−2.45 ppm attributed to benzylic -CH_3 ester remained almost constant (see **Table 2**). Additionally, acetylated samples displayed some peaks at 7.28, 7.38 and 7.75 ppm, attributed to traces of pyridine. In addition, ^{13}C NMR was also used to determine the chemical structure of samples and to confirm the successful modifications of lignin (**Fig. 4b**). It can be observed that the aromatic region of the spectra for kraft lignin (**Table 3**) can be divided into protonated ($C_{Ar–H}$, 121−117 ppm), condensed ($C_{Ar–C}$, 145−121 ppm) and oxygenated aromatic ($C_{Ar–O}$, 153−145 ppm) regions. The C_3 and C_4 carbon atoms on the aromatic ring correspond to the oxygenated aromatic region, whereas the protonated region (117−109 ppm) comprises C_2 and C_6 methine carbon atoms and protonated C_5 carbons [37]. On the other hand, the condensed aromatic region includes C_1 and C_5 carbon atoms from condensation of aromatic ring linkages [38]. The chemical shift of δ_C 61.1 and δ_C 60.1 ppm peaks (C_α and C_γ in β−O−4 in primary hydroxyl groups) was not observed in acetylated samples, suggesting the consumption of hydroxyl groups during modification. The peak at 56 ppm was associated to the methoxyl (-OCH_3) group, and the peaks at 115, 121 and 122 ppm were attributed to the *m*-, *p*- and *o*-aromatic-carbon of methoxyl (-OCH_3) group. New signals appeared in acetylated samples at a chemical shift around 170 and 21 ppm, attributable to the carbonyl ester unit of the acetates and the acetyl -CH_3 groups, respectively [39]. The peaks at 168–170 ppm assigned to the phenolic and the aliphatic esters became broader; this indicated that both groups participated in the esterification. The peak at 151.2 ppm was associated to aromatic-carbon connected with ester. Additionally, acetylated samples displayed some peaks at 136 and 123 ppm attributed to traces of pyridine. Based on the ^1H NMR and ^{13}C NMR results and FTIR spectra, it was proved that lignin was successfully acetylated. Furthermore, a morphological study to evaluate the changes on the physical properties of lignin due to

the esterification process was performed. **Fig. 5** shows selected SEM micrographs of neat lignin and acetylated samples at a magnification of 100x, 1000x and 2000x, respectively. As can be observed, powder of neat lignin is composed of wrinkled and irregular spherical granules or particles (**Fig. 5a, d**), while the 1h acetylated sample displays porous particles with pores distributed over their surfaces. Notably, the morphology of the most acetylated sample is very different, as it is composed of super-structured particles: supramolecular assemblies of lignin into microparticles are observed (**Fig. 5c, f**) [40]. This fact suggests that this acetylation process could achieve supramolecular aggregation of lignin, first into clusters and then into particles. These results confirm that the acetylation process and the subsequent recovery procedure in acidic water has a significant impact on the morphology of samples. Finally, the thermal behavior of neat lignin and acetylated samples was investigated using TGA and DSC analysis (**Fig. 6**). The characteristic parameters such as the temperature for the onset of thermal decomposition ($T_{5\%}$, temperature for the 5 wt.% of mass loss), the temperature at which decomposition rate is maximum (T_{max}), the decomposition temperature range (ΔT), the percentage of non-degraded residue and glass transition temperature (T_g), which were calculated from TGA/DTG and DSC curves, are reported in **Table 4**. As can be observed (**Fig. 6a**), only the neat lignin displays a weight loss of about 3.4 wt.% below 125 ºC, which can be attributed to the evaporation of the adsorbed water as a consequence of hydroxyl groups dehydration [41], confirming their highly hydrophilic character. Derivative thermogravimetry (DTG) curve displays a peak shoulder between 150 and 290 ºC, which may be assigned to the degradation of monomeric compounds from lignin and the degradation of carbohydrates, while the main peak located around 290-390 ºC could be associated to the degradation of carbon-carbon bonds between lignin structural units [29]. However, the acetylated samples show two distinct peaks in the DTG curves. The first peak appears in the range of 125–270 ºC, possibly resulting from the degradation of acetylated moieties, with temperatures for the

maximum decomposition rate at around 195–235 ºC, depending on the DS. The second peak could be mainly attributed to the degradation of carbon-carbon linkages of lignin structural units. The TGA analysis also suggests the effect of acetylated process on the thermal stability of samples. The decomposition temperature increased when the degree of acetylation increased. For example, the $T_{5\%}$ increases from 198 to 221 °C when the degree of acetylation increased from 73 to 90 % (see **Table 4**). This higher thermal stability of the acetylated samples could be attributed to the decrease in the number of remaining hydroxyl groups after acetylation [42]. A similar increase in thermal stability with DS has previously been found for acetylated xylan from hardwood kraft pulp [43]. The DSC analysis of neat lignin and acetylated samples show one main thermal event associated to the glass transition temperature (T_g), as can be observed in **Fig. 6b**. This peak appears shifted to lower temperatures in acetylated samples. This difference could be associated with the presence of the acetyl groups in the biopolymer, increasing the distance between chains and, consequently, the free volume and its mobility [44]. In addition, the reduction of OH groups might decrease the intermolecular interaction, helping to reduce the T_g of acetylated samples. The T_g reduction appears slightly higher when reaction time, i.e., degree of substitution, increases (see **Table 4**). Similar results were found for other chemically-modified lignins [44, 45].

3.2 Influence of the acetylation process on the rheological/tribological properties of lignin dispersions

Steady shear flow curves of lignin dispersions at different reaction times and at 23ºC are illustrated in **Fig. 7a**. As can be observed, the acetylated lignin dispersions display a shear-thinning behaviour, showing a tendency to reach a constant viscosity value at high shear rates, the infinite shear rate viscosity. The shear rate dependence of viscosity fitted the Sisko model quite well ($R^2 > 0.995$):

$$\eta = \kappa\dot{\gamma}^{n-1} + \eta_{\infty} \quad (1)$$

where $\dot{\gamma}$is the shear rate, η is the apparent viscosity, κ is the consistency index, n is the flow index and η_{∞} is the infinite shear rate viscosity. Parameters of the best fit to the Sisko model are shown in **Table 5**. The flow index did not show any significant difference with reaction time. However, both the infinite shear rate viscosity and, especially, the consistency index decreased when the reaction time increased. The shear thinning behaviour of these dispersions could be explained as a particular characteristic of elastic soft solids [46]. Thus, the viscous flow behaviour of these materials could be related to the volume fraction of the dispersed phase, which could be modified by physical and/or chemical interactions between the lignin molecules and oil medium. In this sense, the different viscosity values observed, especially in the low shear rate region for dispersions (higher values for lower reaction times), suggest that the microstructure developed should be completely different. More information about the effect of the acetylated process on the microstructural network formed by the acetylated lignin of the dispersions may be extracted from frequency sweep tests. **Fig. 7b** shows the evolution of SAOS functions with frequency, at 23ºC, within the linear viscoelastic range (LVR), as a function of reaction time. As can be seen, the influence of reaction time on the viscoelasticity of dispersions can be classified into two groups (low and high reaction times). Lower reaction times (1-12h) produced dispersions with a mechanical spectrum characterized by higher values of the storage modulus (G') and a minimum in the loss modulus (G'') at intermediate frequencies. These low times also corresponded to the plateau zone of the mechanical spectrum, which is attributed to the well-known gel-like behaviour of particulate networks [2, 4]. However, higher reaction times (24-72h) resulted in dispersions with a fluid-like behaviour, characterized by higher values of the loss modulus (G'') than the storage modulus (G'), typical of random-coil entanglement

networks. Thus, beyond a critical reaction time (12h), the network structure becomes weaker and hence fluid-like behavior is observed. Furthermore, a plateau region at low frequency in G′ and G'' was observed in the samples with high reaction times (24-72h). There is a spread of G' modulus at low and high frequencies, while the viscous modulus G'' becomes less dependent on the reaction time, especially at high frequencies. Taking into account that the acetylated lignin samples with lower reaction times (6 or 12 h) display a similar degree of substitution than samples processed with higher reaction times, it could be concluded that the differences in the type of microstructural network of the dispersions are due especially to the morphology of acetylated lignin. According to SEM images (see **Fig. 5**), from the size, shape, and surface of the lignin particles, it is suggested that in the reaction processes the Brownian motion and the colloidal forces within the dispersion come into play. The Brownian effects become more important when the particle size is small (higher reaction times). Hence, the Brownian motion tends to make the dispersions viscous-like, while the colloidal forces tend to make the dispersions gel-like.

Based on the results obtained, the acetylated lignin with the lowest reaction time (1 h) could be proposed as a possible thickener candidate to develop semisolid lubricants. Firstly, the physical stability of this type of dispersion against the phase separation was excellent, since there were no syneresis problems or excessive "oil bleeding" after a period of aging (see Fig. 7b). In addition, their mechanical spectrum was similar to commercial multi-use mineral oil- or lithium soap-based lubricating greases [47], as well as other gel-like dispersions based on synthetic polymers [48]. **Fig. 8a** shows the flow curves of dispersions at different concentrations (30-40 wt.%) of acetylated lignin (1h). Flow curves exhibited a shear thinning behaviour, reaching a constant viscosity value at a high shear rate, enabling the estimation of an infinite shear rate viscosity (η_∞). However,

dispersions with higher lignin concentrations showed a fracture of the sample at high shear rate, since a significant decay in the slope of the viscosity is observed. This is not unusual, since viscous flow behaviour of a semisolid lubricant is complex and could present several experimental problems, such as wall-slip, shear-banding, fracture, sample expelling, etc. Again, the shear rate viscosity dependence was fitted to the Sisko model and the parameters obtained from this model are shown in **Table 5**. The consistency index increases with the concentration of acetylated lignin. This increase may be explained by the fact that lignin particles have a significant thickening effect in the bulk phase. **Fig. 8b** shows the mechanical spectra of dispersions as a function of acetylated lignin concentration. Predictably, the values of G' and G'' increased when lignin (thickener) concentration increased, which is indicative of a more entangled microstructural network. This influence on the viscoelastic functions was also analysed by the evolution of the plateau modulus, G^o_N, over lignin content. This modulus is a characteristic parameter of the plateau zone of the mechanical spectrum and it may be defined as the extrapolation of the entanglement contribution to G at high frequencies, which could be approximately calculated from tan (G''/G') as follow [34]:

$$G_N{}^o = [G']_{tan\frac{G''}{G'}\to min} \quad (2)$$

G^o_N values are displayed versus acetylated lignin content in **Fig. 9** for the dispersions together with the corresponding optical microscopy images to shed light on the relationship between rheology and morphology. The G^o_N values increased exponentially with the lignin content, and these data were very well fitted to an exponential model. Optical microscopy results corroborated that the microstructure of these dispersions consists of particles and aggregates. Acetylated lignin yields a significant gel-like behaviour as a consequence of adequate physical properties and strong interaction between lignin particle surfaces and hydrocarbons molecules due to a compatibility of

acetyl group in the vegetable oil. The physical network of the gel-like dispersion becomes stronger as a result of higher particle density (tiny aggregates) which promotes a more entangled network.

Finally, the lubrication properties of these gel-like dispersions were investigated in a ball-on-plate tribological contact. Specific normal load (20 N) and rotational speed (100 rpm) conditions were selected to achieve the mixed lubrication regime, previously determined by performing ramps of rotational speed, i.e., the Stribeck curves. Given the frictional response, a steady-state value for the coefficient of friction was approximately achieved in all cases after 5-6 min, and these values were not dramatically influenced by time in any case. All the values obtained of the coefficient of friction in the steel–steel ball-on-plate configuration were similar to obtained with a lithium commercial lubricating grease, about 0.11±0.012 (see **Fig. 10**) [47]. The topography and size of friction surfaces was also investigated by the optical microscope, as shown in **Fig. 10**. A rounded wear mark appears in all cases and micro-pits and micro-furrow ditches are displayed in the plates after the friction test. As can be observed, the wear diameter decreased when acetylated lignin concentration increased in dispersion.

4. Conclusions

In this work, the influence of the acetylation process of low kraft lignin on rheology, tribology and microstructure of dispersions in castor oil in order to develop an environmentally friendly semisolid lubricant was investigated. From the experimental results obtained, it can be concluded that the apparent viscosity, linear viscoelasticity functions and lubrication properties of dispersions are strongly influenced by the physicochemical properties of the acetylated lignin and its concentration. Lignin was reacted with acetic anhydride in the presence of pyridine as a catalyst by modifying different parameters of the reaction (temperature, ratio of pyridine/acetic anhydride and

time). It was found that an increase of three variables increased the DS up to values that depend on the relationship between their other counterparts and then, a decrease of DS occurs associated with a shift in the reaction equilibrium toward the deacetylation process. The acetylated lignin dispersions showed two different rheological behaviours according to the function of the reaction time: lower reaction times (1-12h) yielded dispersions with a mechanical spectrum characterized by particulate entanglement network typical of gel-like materials, while higher reaction times (24-72h) achieved dispersions with fluid-like properties. This behaviour was attributed to an adequate compatibility between lignin particle surfaces and hydrocarbons molecules of vegetable oil, and, especially, due to the size, morphology, and surface of the lignin particles, which suggests that in the dispersed phase, Brownian motion or colloidal forces come into play depending on the morphological properties of acetylated lignin. Apparent viscosity and viscoelasticity functions increased with the acetylated lignin concentration due to a stronger physical network because of higher particle densities and particle aggregates. According to the lubrication properties, the dispersions in the mixed lubrication regime showed values of the coefficient of friction similar to those obtained with other traditional lubricating greases. From the results obtained, it can be deduced that the acetylation process is a key issue to modulate the rheological properties of dispersions, and the acetylated lignin with a medium degree of substitution and adequate morphological properties can be potentially used as an effective thickener agent to develop semisolid lubricant formulations.

Acknowledgments

This work is part of two research projects, RTI2018-096080-B-C21 and 802C1800001, funded by a Ministerio de Ciencia e Innovación and Junta de Andalucía Spanish programmes, respectively. The authors gratefully acknowledge the financial support.

References

[1] M. Yang, S. Fan, H. Huang, Y. Zhang, Z. Huang, H. Hu, J. Liang, Microwave-assisted selective acetylation of Kraft lignin: Acetic acid as a sustainable reactant for lignin valorization, Int. J. Biol. Macromol. 156 (2020) 280-288.

[2] J.E. Martín-Alfonso, M.J. Martín-Alfonso, J.M. Franco, Tunable rheological-tribological performance of "green" gel-like dispersions based on sepiolite and castor oil for lubricant applications, Appl. Clay Sci. 192 (2020) 105632.

[3] A.Ch. Opia, A.H. Mohd Kameil, S. Syahrullail, Ch.A. Johnson, M. Izhari Izmi, Ch.D. Zul Hilmi, A.B. Abd Rahim, Eichhornia crassipes nanoparticles as a sustainable lubricant additive: Tribological properties optimization and performance under boundary lubrication regime, Ind. Crops Prod. 175 (2022) 114252.

[4] J.E. Martín-Alfonso, M.J. Martín-Alfonso, C. Valencia, M.T. Cuberes. Rheological and tribological approaches as a tool for the development of sustainable lubricating greases based on nano-montmorillonite and castor oil, Friction 9 (2021) 415–428.

[5] L. Mu, J. Wu, L. Matsakas, M. Chen, U. Rova, P. Christakopoulos, J. Zhu, Y. Shi, Two important factors of selecting lignin as efficient lubricating additives in poly (ethylene glycol): Hydrogen bond and molecular weight, Int. J. Biol. Macromol. 129 (2019) 564-570.

[6] A.M. Borrero-López, R. Martín-Sampedro, D. Ibarra, C. Valencia, M.E. Eugenio, J.M. Franco, Evaluation of lignin-enriched side-streams from different biomass conversion processes as thickeners in bio-lubricant formulations, Int. J. Biol. Macromol. 162 (2020) 1398–1413.

[7] E. Cortés-Trivino, C. Valencia, M.A. Delgado, J.M. Franco, Modification of alkali lignin with poly (ethylene glycol) diglycidyl ether to be used as a thickener in biolubricant formulations, Polymers 2018; 10: E670.

[8] D. Tang, X. Huang, W. Tang, Y. Jin, Lignin-to-chemicals: application of catalytic hydrogenolysis of lignin to produce phenols and terephthalic acid via metalbased catalysts, Int. J. Biol. Macromol. 190 (2021) 72–85.

[9] Prakram Singh Chauhan, Ruchi Agrawal, Alok satlewal, Ravindra Kumar, Ravi P. Gupta, S.S.V. Ramakumar. Next generation applications of lignin derived commodity products, their life cycle, techno-economics and societal analysis, Int. J. Biol. Macromol. 197 (2022) 179–200.

[10] G.F. De Gregorio, R. Prado, C. Vriamont, X. Erdocia, J. Labidi, J.P. Hallett, T. Welton, Oxidative depolymerization of lignin using a novel polyoxometalate-protic ionic liquid system, ACS Sustain. Chem. Eng. 4 (2016) 6031-6036.

[11] A.J. Ragauskas, G.T. Beckham, M.J. Biddy, R. Chandra, F. Chen, M.F. Davis, B.H. Davison, R.A. Dixon, P. Gilna, M. Keller, P. Langan, A.K. Naskar, J.N. Saddler, T.J. Tschaplinski, G.A. Tuskan, Ch.E. Wyman. Lignin valorization: improvinglignin processing in the biorefinery, Science 344 (2014) 1–10.

[12] Y. Zhang, H. Pang, D. Wei, J. Lia, S. Li, X. Lina, F. Wang, B. Liao, Preparation and characterization of chemical grouting derived from lignin epoxy resin. Eur. Polym. J. 118 (2019) 290-305.

[13] M.A. Jedrzejczyk, S. Van den Bosch, J. Van Aelst, K. Van Aelst, P.D. Kouris, M. Moalin, Guido R. M. M. Haenen, M.D. Boot, Emiel J. M. Hensen, B. Lagrain, Bert F. Sels, Katrien V. Bernaerts, Lignin-based additives for improved thermo-oxidative stability of biolubricants, ACS Sustain. Chem. Eng. 37 (2021) 12548–12559.

[14] Y. Li, S. Sarkanen, Alkylated Kraft lignin-based thermoplastic blends with aliphatic polyesters, Macromolecules 35 (2002) 9707–9715.

[15] Xiao Jiang, Zhongjian Tian, Xingxiang Ji, Hao Ma, Guihua Yang, Ming He, Lin Dai, Ting Xu, Chuanling Si, Alkylation modification for lignin color reduction and molecular weight adjustment, Int. J. Biol. Macromol. 201 (2022) 400–410.

[16] P. Buono, A. Duval, P. Verge, L. Averous, Y. Habibi, New insights on the chemical modification of lignin: acetylation versus silylation, ACS Sustain. Chem. Eng. 4 (2016) 5212–5222.

[17] K.A.Y. Koivu, H. Sadeghifar, P.A. Nousiainen, D.S. Argyropoulos, J. Sipilä, Effect of fatty acid esterification on the thermal properties of softwood kraft lignin, ACS Sustain. Chem. Eng. 4 (2016) 5238–5247.

[18] F. Monteil-Rivera, L. Paquet, Solvent-free catalyst-free microwave-assisted acylation of lignin, Ind. Crop. Prod. 65 (2015) 446–453.

[19] D.R. de Oliveira, I. de M. Nogueira, F.J.N. Maia, M.F. Rosa, S.E. Mazzetto, D. Lomonaco, Ecofriendly modification of acetosolv lignin from oil palm biomass for improvement of PMMA thermo-oxidative properties, J. Appl. Polym. Sci. 134 (2017) 1–8.

[20] Tripathi, M. Ago, S.A. Khan, O.J. Rojas, Heterogeneous acetylation of plant fibers into micro- and nanocelluloses for the synthesis of highly stretchable, tough, and water-resistant co-continuous filaments via wet-spinning, ACS Appl. Mater. Interfaces. 10 (2018) 44776–4478.

[21] T. Joffre, K. Segerholm, C. Persson, S.L. Bardage, C.L. Luengo Hendriks, P. Isaksson, Characterization of interfacial stress transfer ability in acetylation-treated wood fibre composites using X-ray microtomography, Ind. Crops Prod. 95 (2017) 43–49.

[22] R. Fang, X. Cheng, W.S. Lin, Preparation and application of dimer acid/lignin graft copolymer, Bioresources 6 (2011) 2874–2884.

[23] Y. Teramoto, S.H. Lee, T. Endo, Phase structure and mechanical property of blends of organosolv lignin alkyl esters with poly (ε-caprolactone), Polym. J. 41 (2009) 219–227.

[24] K. Shayesteh, G. Mohammadzadeh, M. Zamanloo, Study and optimization of parameters affecting the acetylation process of lignin sulfonate biopolymer, Int. J. Biol. Macromol. 163 (2020) 1810-1820.

[25] D. Rabelo de Oliveira, F. Avelino, S. Elaine Mazzetto, D. Lomonaco, Microwave-assisted selective acetylation of Kraft lignin: Acetic acid as a sustainable reactant for lignin valorization, Int. J. Biol. Macromol. 164 (2020) 1536-1544.

[26] M. Borrego, J.E. Martín-Alfonso, M.C. Sánchez, C. Valencia, J.M. Franco, Electrospun lignin-PVP nanofbers and their ability for structuring oil. Int. J. Biol. Macromol. 180 (2021) 212–221.

[27] E.J. Delaney, L.E. Wood, I.M. Klotz, Poly(ethylenimines) with alternative (alkylamino)pyridines as nucleophilic catalysts. J. Am. Chem. Soc. 104 (1982) 799–807.

[28] X. Zhao, Z. Huang, Y. Zhang, M. Yang, D. Chen, K. Huang, H. Hu, A. Huang, X. Qin, Z. Feng, Efficient solid-phase synthesis of acetylated lignin and a comparison of the properties of different modified lignins. J. Appl. Polym. Sci. 134 (2017) 44276.

[29] F. Hernandez-Ramos, M. Gonzalez Alriols, T. Calvo-Correas, J. Labidi, X. Erdocia, Renewable biopolyols from residual aqueous phase resulting after lignin precipitation, ACS Sustain. Chem. Eng. 9 (2021) 3608–3615.

[30] T. Xiao, H. Yuan, Q. Ma, X. Guo, Y. Wu, An approach for in situ qualitative and quantitative analysis of moisture adsorption in nanogram-scaled lignin by using micro-FTIR spectroscopy and partial least squares regression, Int. J. Biol. Macromol. 132 (2019) 1106-1111.

[31] J. Fernandez-Rodríguez, X. Erdocia, C. Sánchez, A. González Alriols, J. Labidi, Lignin depolymerization for phenolic monomers production by sustainable processes. J. Energy Chem. 26 (2017) 622−631.

[32] M. Gilarranz, F. Rodriguez, M. Oliet, J. Garcia, V. Alonso, Phenolic OH group estimation by FTIR and UV spectroscopy. Application to organosolv lignins. J. Wood Chem. Technol. 21 (2001) 387–395.

[33] J.C. Onwuka, E.B. Agbaji, V.O. Ajibola, F.G. Okibe, Thermodynamic pathway of ligno-cellulosic acetylation process, BMC Chem. 13 (2019) 1-11.

[34] N. Cachet, S. Camy, B. Benjelloun-Mlayah, J-S. Condoret, M. Delmas, Esterification of organosolv lignin under supercritical conditions. Ind. Crops Prod. 58 (2014) 287-297.

[35] X. Zhao, Y. Zhang, L. Wei, H. Hu, Z. Huang, M. Yang, A. Huang, J. Wu, Z. Feng, Esterification mechanism of lignin with different catalysts based on lignin model compounds by mechanical activation-assisted solid-phase synthesis. RSC Adv. 7 (2017) 52382-52390.

[36] Lundquist, K. Proton (1H) NMR Spectroscopy. In Methods in Lignin Chemistry; Lin, S. Y., Dence, C. W., Eds.; Springer-Verlag:Berlin-Heidelberg, 1992.

[37] X. He, F. Luzi, W. Yang, Z. Xiao, L. Torre, Y. Xie, D. Puglia, Citric Acid as green modifier for tuned hydrophilicity of surface modified cellulose and lignin nanoparticles. ACS Sustainable Chem. Eng. 6 (2018) 9966−9978.

[38] S.S. Nair, S. Sharma, Y. Pu, Q. Sun, S. Pan, J.P. Zhu, Y. Deng, A.J. Ragauskas, High shear homogenization of lignin to nanolignin and thermal stability of nanolignin-polyvinyl alcohol blends. ChemSusChem 7 (2014) 3513−3520.

[39] J.L. Wen, B.L. Xue, S.L. Sun, R.C. Sun, Quantitative structure characterization and thermal properties of birch lignins after auto-catalyzed organosolv pretreatment and enzymatic hydrolysis. J. Chem. Technol. Biot. 88 (2013) 1663-1671.

[40] M. Ago, B.L. Tardy, L. Wang, J. Guo, A. Khakalo, O.J. Rojas. Supramolecular assemblies of lignin into nano- and microparticles, MRS Bull. 42, 371-378 (2017).

[41] S. Laurichesse and L. Avérous, Chemical modification of lignins: Towards biobased polymers, Prog. Polym. Sci. 39, 1266–1290 (2014).

[42] J. Aburto, I. Alric, S. Thiebaud, E. Borredon, D. Bikiaris, J. Prinos, C. Panayiotou, Synthesis, characterization, and biodegradability of fatty-acid esters of amylose and starch. J. Appl. Polym. Sci. 74 (1999) 1440–1451.

[43] N.G.V. Fundador, Y. Enomoto-Rogers, A. Takemura, T. Iwata, Acetylation and characterization of xylan from hardwood kraft pulp. Carbohydr. Polym. 87 (2012) 170-176.

[44] J. Rocha Gouveiaa, R. Ramos de Sousa Júnior, A. Orzari Ribeiro, S.A. Saraiva, D. Jackson dos Santos. Effect of soft segment molecular weight and NCO:OH ratio on thermomechanical properties of lignin-based thermoplastic polyurethane adhesive, Eur. Polym. J. 131 (2020) 109690.

[45] L. Dehne, C. Vila Babarro, B. Saake, K.U. Schwarz, Influence of lignin source and esterification on properties of lignin-polyethylene blends, Ind. Crops Prod. 86 (2016) 320–328.

[46] J. Hermoso, F. Martinez-Boza, C. Gallegos, Influence of viscosity modifier nature and concentration on the viscous flow behaviour of oil-based drilling fluids at high pressure, Appl. Clay Sci. 87 (2014) 14-21.

[47] J.E. Martín-Alfonso, F. López-Beltrán, C. Valencia, J.M. Franco, Effect of an alkali treatment on the development of cellulose pulp-based gel-like dispersions in vegetable oil for use as lubricants. Tribol. Int. 123 (2018) 329–336.

[48] J.E. Martín-Alfonso, J.M. Franco, Ethylene-vinyl acetate copolymer (EVA)/sunflower vegetable oil polymer gels: Influence of vinyl acetate content, Polym. Test. 37 (2014) 78–85.

Figure Captions

Figure 1. Catalytic mechanism of esterification: (a) activation of acid anhydride by pyridine, (b) acetylation of aromatic of alcohol, (c) acetylation of aliphatic of alcohol.

Figure 2. FTIR spectra of neat lignin and acetylated samples prepared at temperature of 30 °C and ratio of pyridine/acetic anhydride (1/3) as a function of reaction time.

Figure 3. Evolution of the substitution degree with processing variables of acetylation: (a) reaction temperature, (b) ratio of pyridine/acetic anhydride and (c) reaction time. Normalized transmittance area for aliphatic and aromatic C=O ester groups ($A_{C=O\ (ester)}/A_{ref}$) was included for a better understanding of the evolution of acetylation process.

Figure 4. ^{1}H NMR (a) and ^{13}C NMR (b) spectra of neat lignin and acetylated samples as a function of reaction time.

Figure 5. SEM micrographs of selected samples: (a, d) neat lignin (x100 and x1000), (b, e) acetylated 1 h (x100 and x1000) and (c, f) acetylated 72 h (x100 and x1000).

Figure 6. Thermal behavior of neat lignin and acetylated samples as a function of reaction time: (a) TGA thermograms/DTG curves and (b) DSC curves.

Figure 7. Rheological behavior of dispersions as a function of reaction time: (a) Steady shear flow curves. Solid lines represent fits to the Sisko model with the parameters given in **Table 2**. (b) Frequency sweep test performed within the linear viscoelastic range of the soft materials.

Figure 8. Rheological behavior of dispersions as a function of acetylated lignin concentration: (a) Steady shear flow curves. Solid lines represent fits to the Sisko model

with the parameters given in **Table 2**. (b) Frequency sweep test performed within the linear viscoelastic range of the soft materials.

Figure 9. Plateau modulus as a function of acetylated lignin concentration in the (30-40) wt.% range. Optical images have been included to shed light of the relationship between their morphology and rheological properties.

Figure 10. Friction coefficient and wear diameter obtained by applying a constant rotational speed of 100 rpm and a 20 N normal load at 23ºC. Optical images of the worn plate surface for steel/steel contacts have been included.

a)

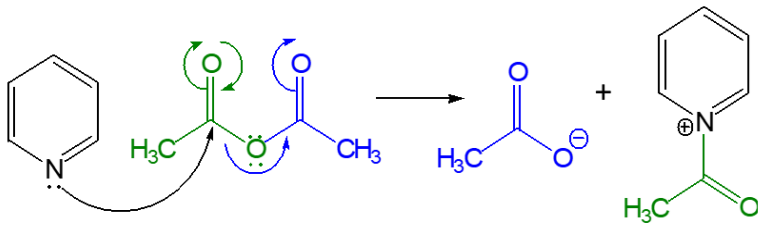

b)

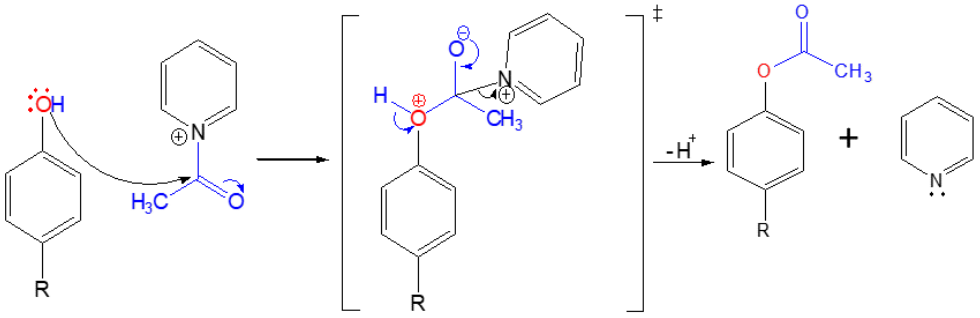

c)

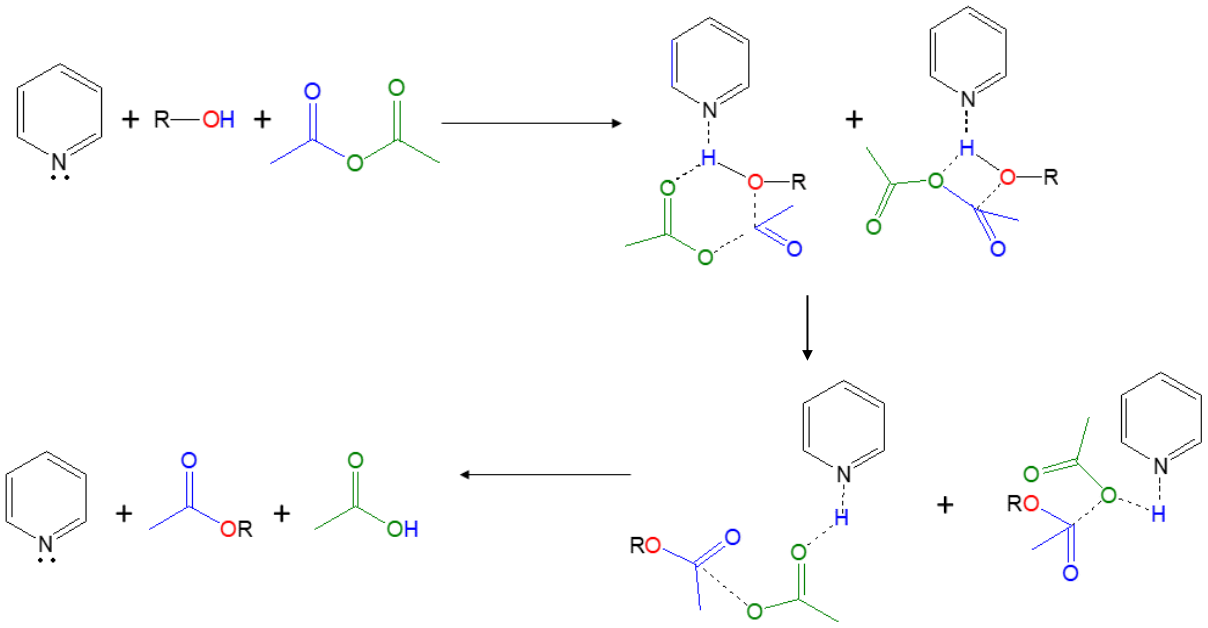

Figure 1.

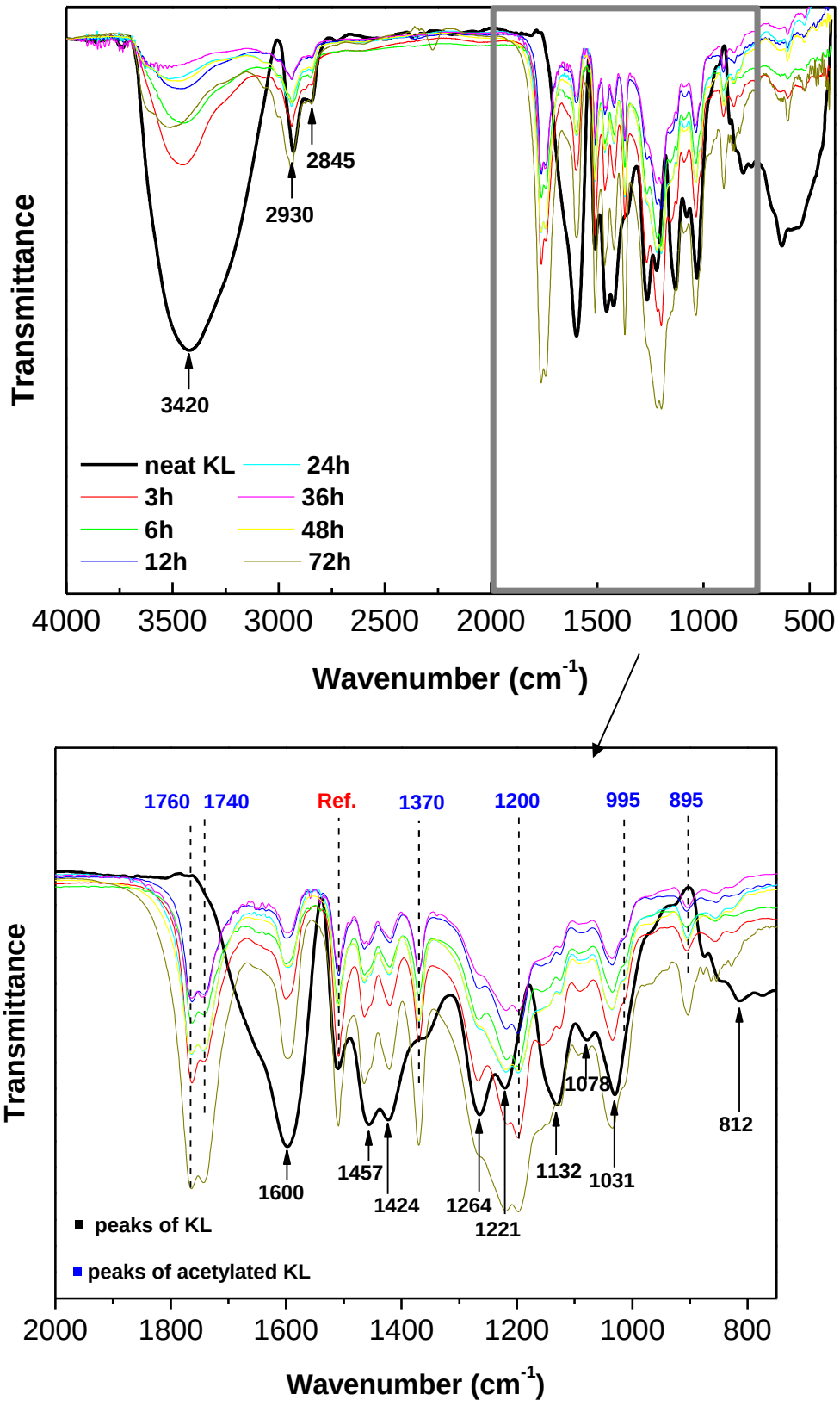
Transmittance
3420
2930
2845
neat KL
3h
6h
12h
24h
36h
48h
72h
4000
3500
3000
2500
2000
1500
1000
500
Wavenumber (cm-1)
1760
1740
Ref.
1370
1200
995
895
1600
1457
1424
1264
1221
1132
1078
1031
812
peaks of KL
peaks of acetylated KL
2000
1800
1600
1400
1200
1000
800
Wavenumber (cm-1)

Figure 2.

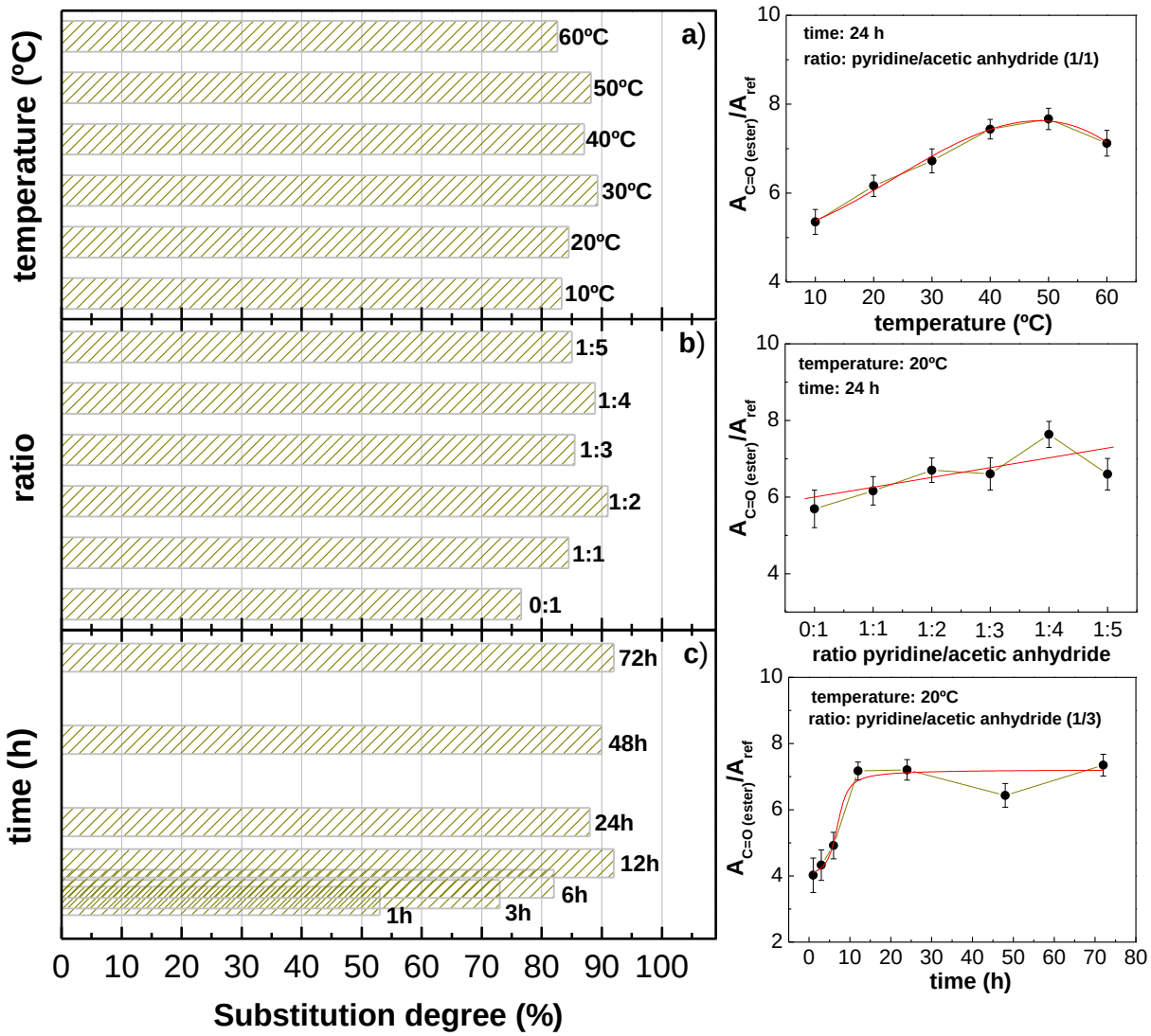
temperature (°C)
ratio
time (h)
a)
b)
c)
60°C
50°C
40°C
30°C
20°C
10°C
1:5
1:4
1:3
1:2
1:1
0:1
72h
48h
24h
12h
6h
3h
1h
0 10 20 30 40 50 60 70 80 90 100
Substitution degree (%)
time: 24 h
ratio: pyridine/acetic anhydride (1/1)
A C=O (ester) /A ref
temperature (°C)
temperature: 20°C
time: 24 h
ratio pyridine/acetic anhydride
temperature: 20°C
ratio: pyridine/acetic anhydride (1/3)
time (h)

Figure 3.

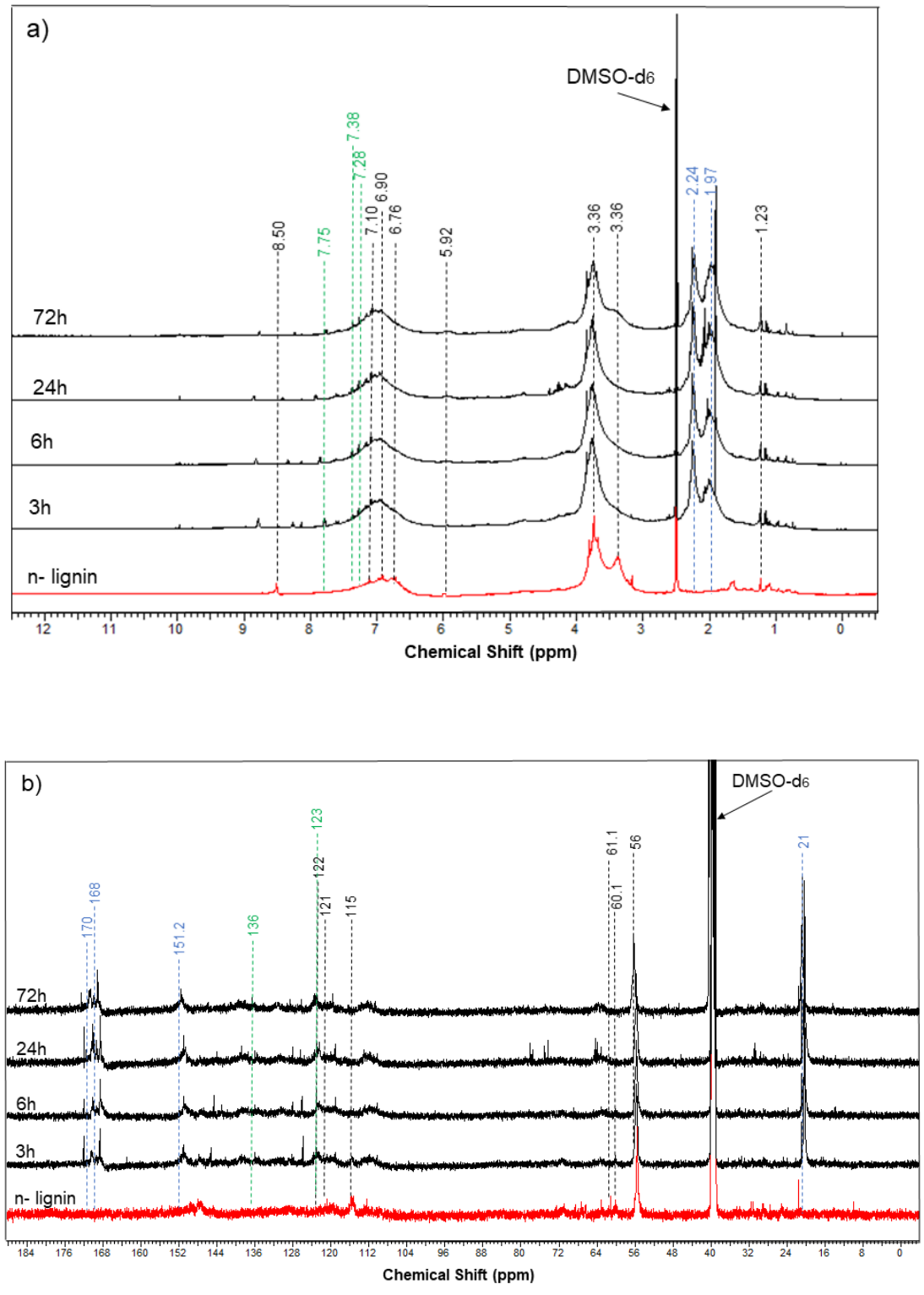
a)
DMSO-d6
8.50
7.75
7.38
7.28
7.10
6.90
6.76
5.92
3.36
3.36
2.24
1.97
1.23
72h
24h
6h
3h
n- lignin
Chemical Shift (ppm)
b)
DMSO-d6
170
168
151.2
136
123
122
121
115
61.1
60.1
56
21
72h
24h
6h
3h
n- lignin
Chemical Shift (ppm)

Figure 4.

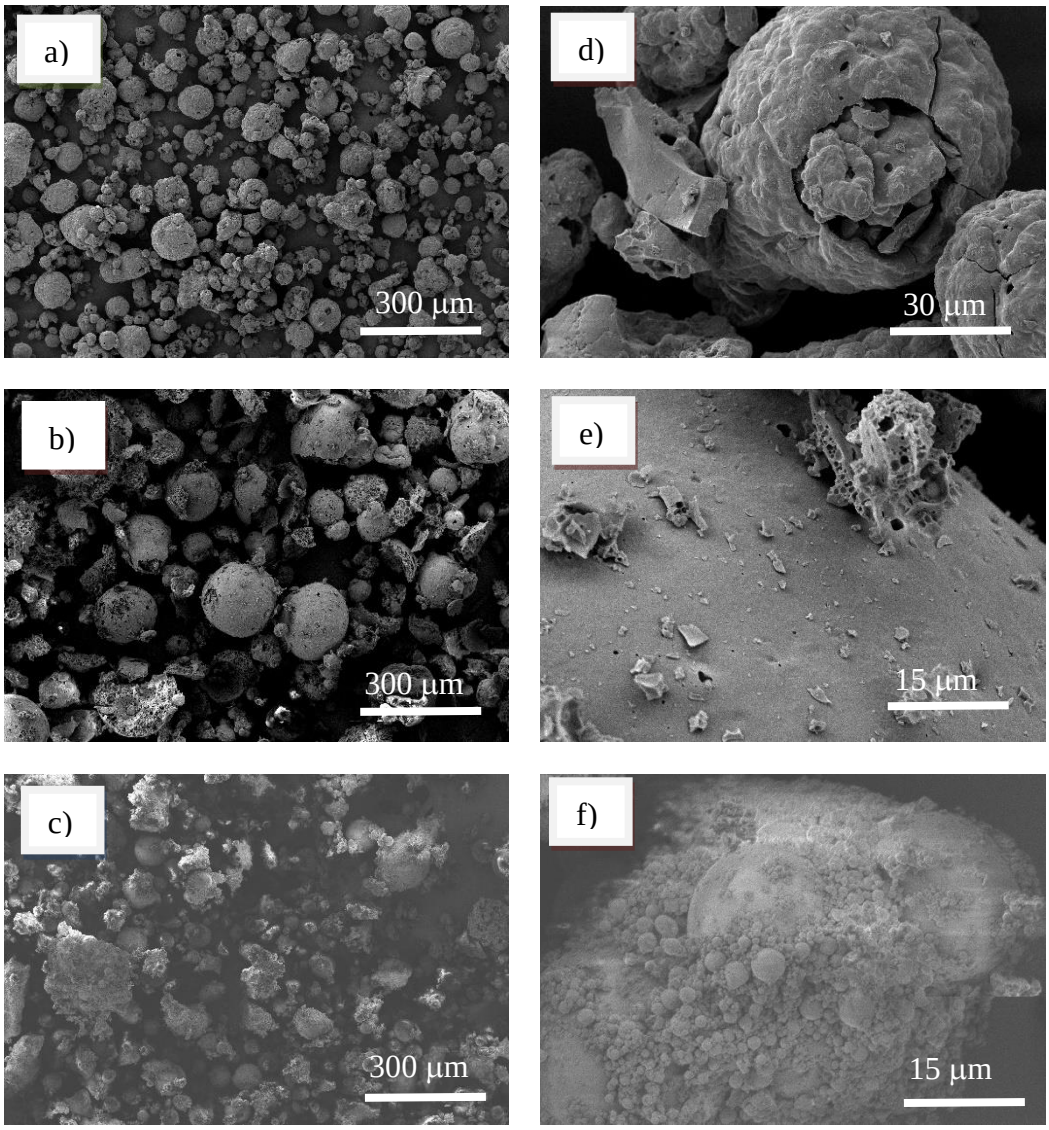

Figure 5.

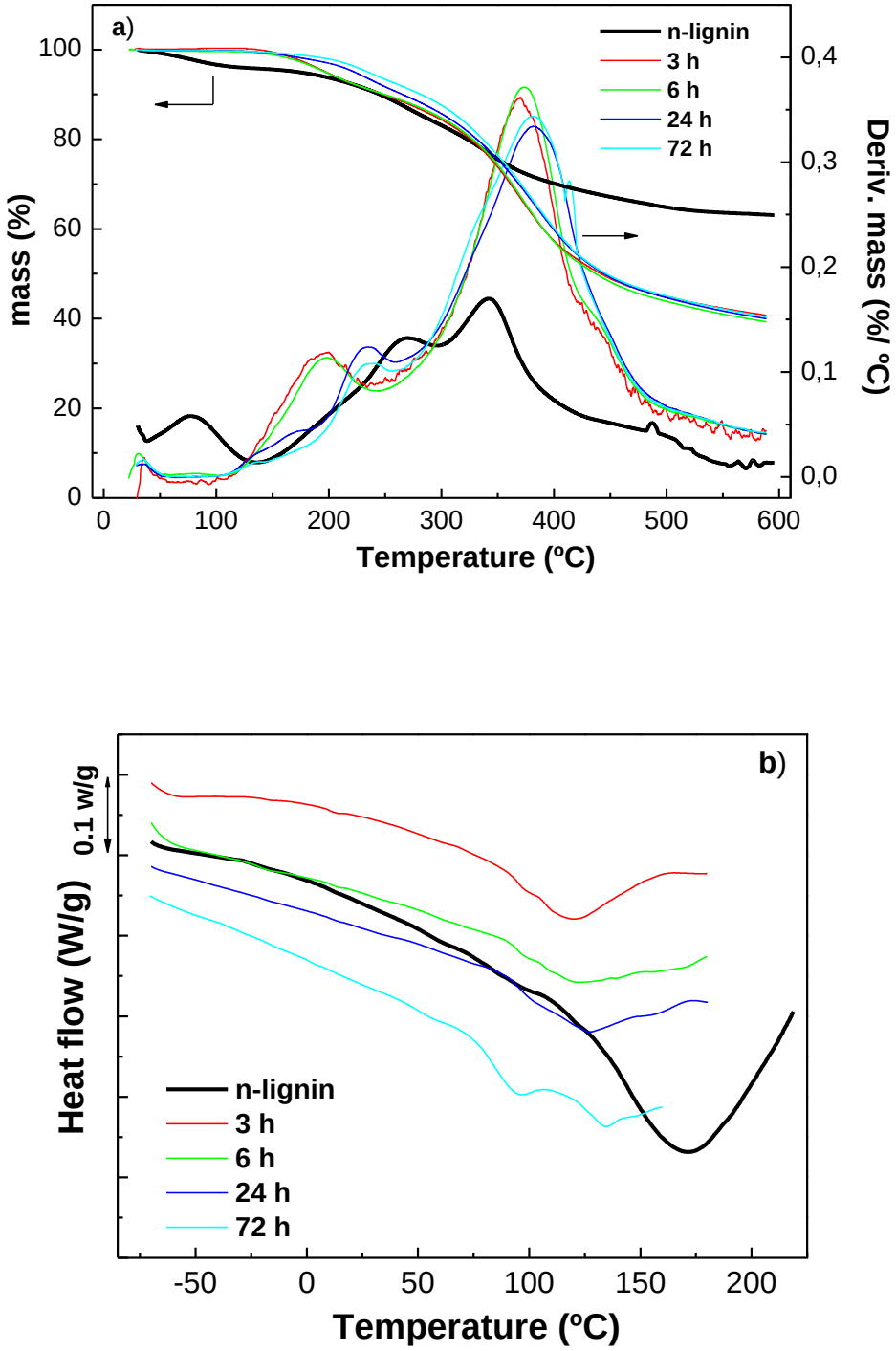
a)
n-lignin
3 h
6 h
24 h
72 h
mass (%)
Deriv. mass (%/ °C)
Temperature (°C)
b)
0.1 w/g
Heat flow (W/g)
n-lignin
3 h
6 h
24 h
72 h
Temperature (°C)

Figure 6.

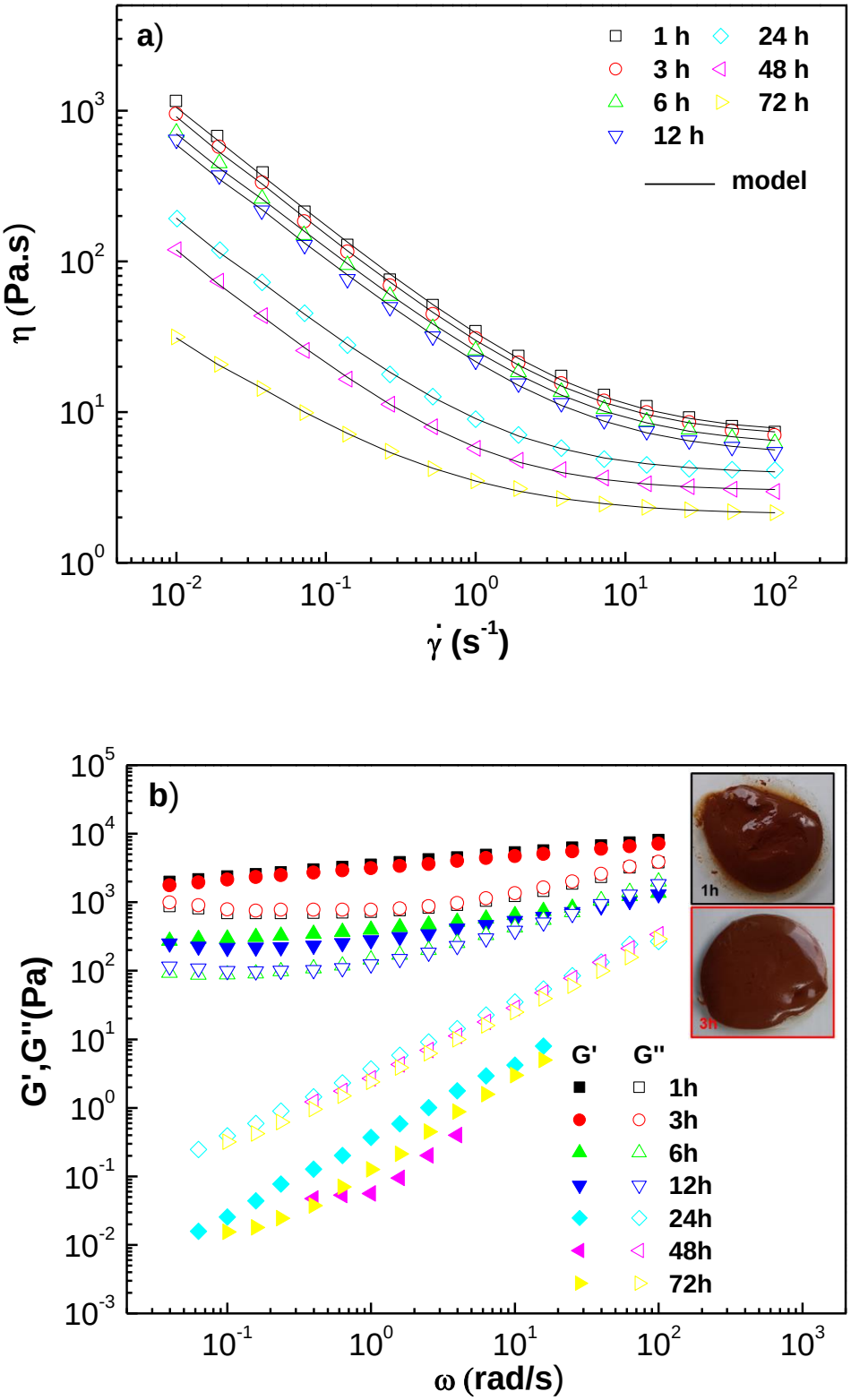
a)
1 h
3 h
6 h
12 h
24 h
48 h
72 h
model
η (Pa.s)
γ̇ (s-1)
b)
G',G''(Pa)
ω (rad/s)
G'
G''
1h
3h
6h
12h
24h
48h
72h

Figure 7.

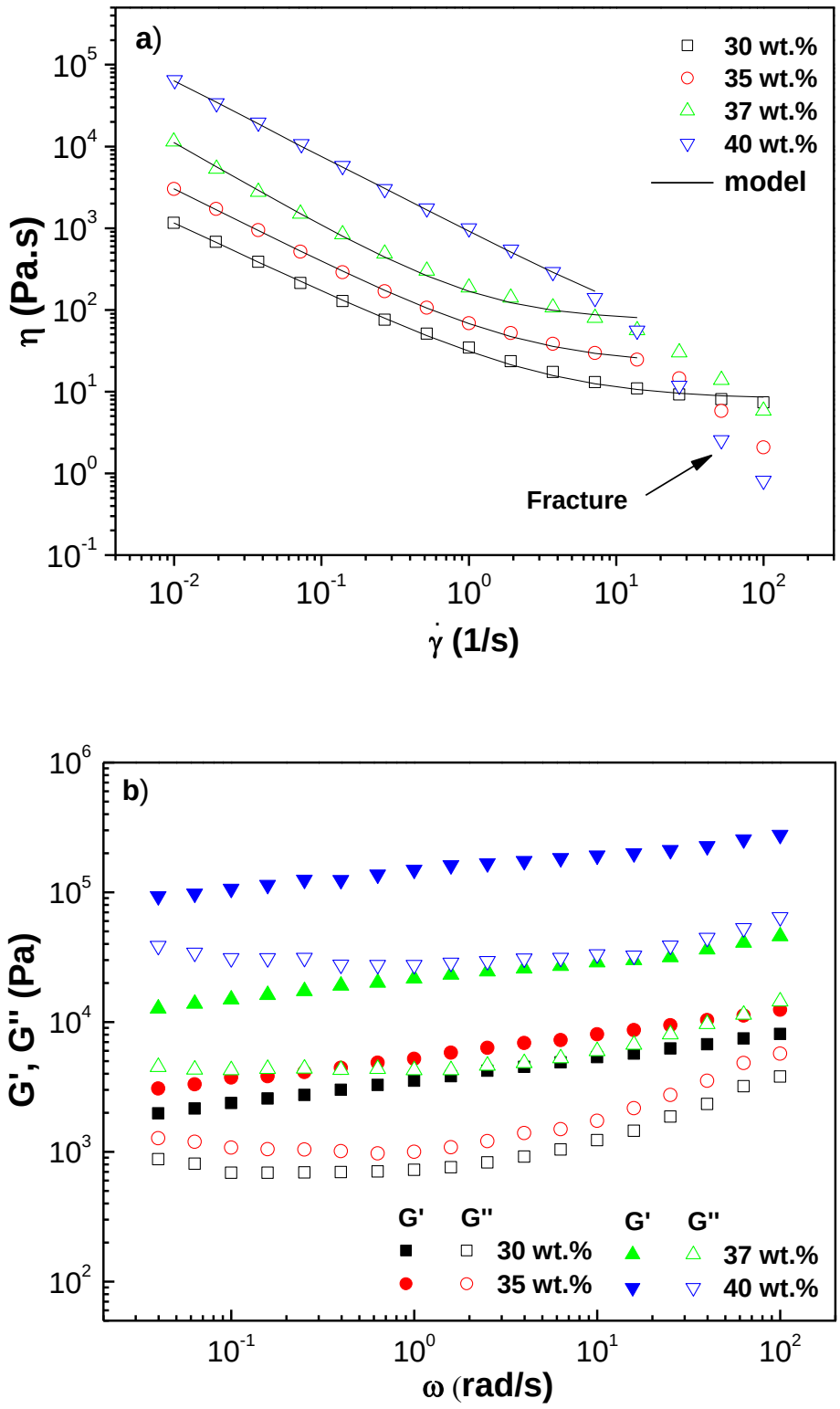
a)
30 wt.%
35 wt.%
37 wt.%
40 wt.%
model
Fracture
η (Pa.s)
γ̇ (1/s)
b)
G', G'' (Pa)
G'
G''
30 wt.%
35 wt.%
37 wt.%
40 wt.%
ω (rad/s)

Figure 8.

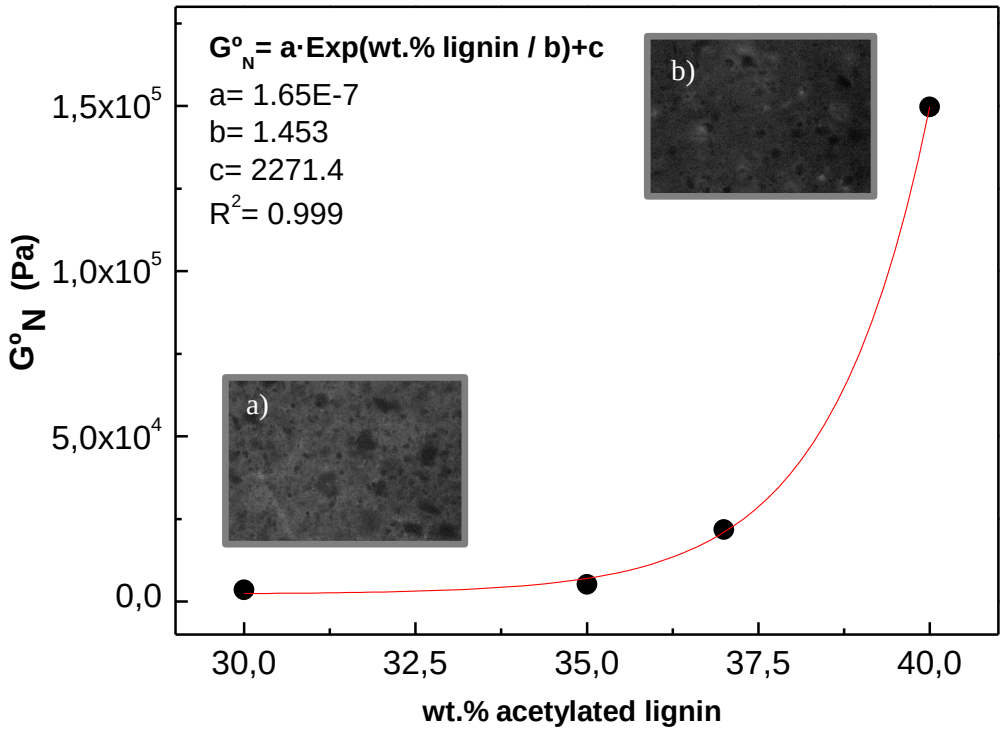
G°N= a·Exp(wt.% lignin / b)+c
a= 1.65E-7
b= 1.453
c= 2271.4
R2= 0.999
b)
a)
G°N (Pa)
1,5x10^5
1,0x10^5
5,0x10^4
0,0
30,0
32,5
35,0
37,5
40,0
wt.% acetylated lignin

Figure 9.

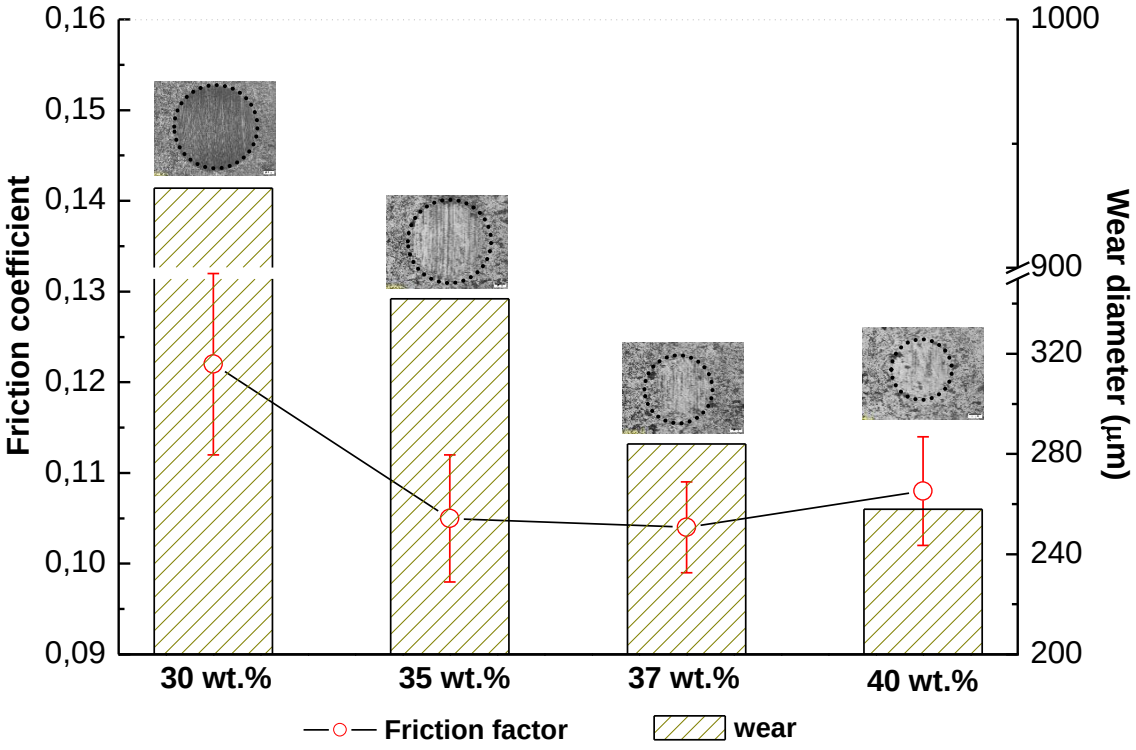
0,16
0,15
0,14
0,13
0,12
0,11
0,10
0,09
Friction coefficient
1000
900
320
280
240
200
Wear diameter (μm)
30 wt.%
35 wt.%
37 wt.%
40 wt.%
Friction factor
wear

Figure 10

Table 1

Main FTIR bands assignment of the neat lignin and acetylated samples

Band position (cm^{-1})	**Assignment**
3420	O-H stretching of aromatic and aliphatic OH groups
2930	C-H asymmetric and symmetric vibration of methyl/methylene groups
2845	C-H asymmetric and symmetric vibration of methyl/methylene groups/C-H stretching in O-CH_3 groups
1760	C=O stretch of aromatic acetyl groups
1740	C=O stretch of aliphatic acetyl groups
1600	Aromatic skeletal vibration
1510 (ref)	Aromatic skeletal vibration
1457	O-CH_3 deformation, C-H deformation asymmetric in CH_3 and CH_2
1424	Aromatic skeletal vibration with C-H in-plane deformation
1370	C-H of aliphatic chain, acetoxy CH_3 bending
1264	C-H of plane vibrations of guaiacyl (G-units)
1221	C-O-C of guaiacyl ring (G-units) (phenolic groups)
1200	C-O-C of aromatic acetyl groups
1132	C-H of syringyl (S-units)
1121	Aromatic C-H in plane deformation (S-units), characteristic band of acetic anhydride
995	Characteristic band of acetic anhydride
895	Characteristic band of acetic anhydride
812	C-H of plane vibrations of guaiacyl (G-units)

Table 2

Signals assignment and integral of neat lignin and acetylated samples in the ^{1}H NMR spectrum

Chemical Shift (ppm)	Assignment	Integral					
		3h	6h	12h	24h	48h	72h
1.23	$-CH_3$						
1.70 – 2.10	$-CH_3$ aliphatic ester	0.10	0.12	0.15	0.17	0.15	0.16
2.1 – 2.5	$-CH_3$ aromatic ester	0.10	0.11	0.11	0.12	0.11	0.11
3.00 – 3.50	Aliphatic -OH						
3.50 – 4.10	Methoxyl ($-OCH_3$)						
5.80 – 6.00	H_α and H_β in β-O-4 linked to C_4 phenyl propane						
6.00 – 6.80	$C_{2,6}$-$H_{2,6}$ in S-units						
6.80 – 7.00	$C_{2,5,6}$-$H_{2,5,6}$ in G-units						
7.00 – 7.50	$C_{2,6}$-$H_{2,6}$ in H-units						
7.28	$C_{3,5}$-$H_{3,5}$ in pyridine						
7.38	C_4-H_4 in pyridine						
7.75	$C_{2,6}$-$H_{2,6}$ in pyridine						
8.50	Phenolic -OH						

Table 3

Signals assignment of neat lignin and acetylated samples in the ^{13}C NMR spectrum

Chemical Shift (ppm)	Assignment
21.0	Acetyl (-CH_3)
56.0	Methoxyl (-OCH_3)
60.1	C_γ in β-O-4 in primary -OH groups
61.1	C_α in β-O-4 in primary -OH groups
109.0 – 117.0	C_2 and C_6 methine carbon atoms and C_5
117.0 – 121.0	$C_{Ar\text{-}H}$
121.0 – 145.0	$C_{Ar\text{-}C}$
115.0	*m*-aromatic-carbon linked to -OCH_3 group
121.0	*p*-aromatic-carbon linked to -OCH_3 group
122.0	*o*-aromatic-carbon linked to -OCH_3 group
123.0	$C_{3,5}$ in pyridine
136.0	C_4 in pyridine
145.0 – 153.0	$C_{Ar\text{-}O}$
151.2	C_{Ar} connected with ester
168.0	C carbonyl phenolic ester
170.0	C carbonyl aliphatic ester

Table 4

Thermal characteristic parameters of neat lignin and acetylated samples obtained by TGA and DSC analysis

Samples	$T_{5\%}$ (ºC)	T_{max} (ºC)	ΔT (ºC)	residue (%)	T_g (ºC)
neat lignin	171	268/341	358	36.9	144.6
1 h	185	199/350	330	56.3	108.0
3 h	198	198/370	314	59.2	104.6
6 h	205	198/374	306	60.7	94.8
12 h	223	228/382	297	58.8	78.9
24 h	220	235/382	286	60.0	98.4
48 h	221	231/378	297	60.9	88.7
72 h	222	235/381	292	59.6	80.3

Table 5

Fitting parameters according to the Sisko model for dispersion as a function of reaction time and lignin concentration.

Reaction time	m (Pa s^n)	n	η_∞ (Pa s)
1 h	26.27	0.201	7.19
3 h	23.12	0.203	6.81
6 h	19.52	0.222	5.95
12 h	16.42	0.221	5.18
24 h	5.154	0.214	3.89
48 h	2.857	0.199	2.99
72 h	1.403	0.342	2.08
Lignin content			
30 wt.%	26.27	0.201	7.19
35 wt.%	46.20	0.101	21.7
37 wt.%	94.19	0.087	34.1
40 wt.%	891.7	0.071	26.5